



HAL
open science

Numerical and Experimental Investigation of Combustion Regimes in a Dual Fuel Engine

Haïfa Belaid-Saleh, Stéphane Jay, Julian Kashdan, Cyprien Ternel, Christine
Mounaïm-Rousselle

► **To cite this version:**

Haïfa Belaid-Saleh, Stéphane Jay, Julian Kashdan, Cyprien Ternel, Christine Mounaïm-Rousselle. Numerical and Experimental Investigation of Combustion Regimes in a Dual Fuel Engine. 11th International Conference on Engines & Vehicles: ICE 2013, 2013, Rome, Italy. SAE Paper 2013-24-0015, 10.4271/2013-24-0015 . hal-00920703

HAL Id: hal-00920703

<https://hal.science/hal-00920703>

Submitted on 8 Dec 2022

HAL is a multi-disciplinary open access archive for the deposit and dissemination of scientific research documents, whether they are published or not. The documents may come from teaching and research institutions in France or abroad, or from public or private research centers.

L'archive ouverte pluridisciplinaire **HAL**, est destinée au dépôt et à la diffusion de documents scientifiques de niveau recherche, publiés ou non, émanant des établissements d'enseignement et de recherche français ou étrangers, des laboratoires publics ou privés.



Distributed under a Creative Commons Attribution - NonCommercial 4.0 International License

Numerical and Experimental Investigation of Combustion Regimes in a Dual Fuel Engine

Haifa Belaid-Saleh

Université d'Orléans and IFPEN

Stéphane Jay, Julian Kashdan and Cyprien Ternel

IFP Energies Nouvelles

Christine Mounaïm-Rousselle

Université d'Orléans

ABSTRACT

Among the new combustion concepts envisaged to meet future regulations, the Dual Fuel (DF) concept is considered to be an attractive strategy due to its potential to reduce CO₂ emissions and engine-out pollutant emissions levels. A small quantity of high-cetane fuel (Diesel) is injected in the combustion chamber in order to ignite a homogeneous mixture of air and a highly volatile fuel (gasoline in our study). The DF concept has been shown to achieve improved engine thermal efficiency and low engine-out NO_x and soot emissions. However, the physical mechanisms controlling DF combustion and in particular, determination of the predominant combustion regime(s) are not yet well understood. In this study, numerical simulations (CFD) and optical engine measurements are used to investigate Dual Fuel combustion. The ECFM3Z combustion model (implemented in the IFP-C3D code) is presented in this paper in addition to preliminary results which have been performed for DF internal combustion (IC) engine simulations. The approach employed in this study allowed determination of the relative contributions of auto-ignition (AI), flame propagation (ECFM) and Burned Gas (BG) to the total heat release and combustion development in terms of the spatio-temporal evolution throughout the engine cycle. The objective is first of all to evaluate the capacity/potential of existing models to cope with the various combustion regimes that might exist in DF combustion strategies and in particular transitions between different combustion modes. Results of preliminary

experiments on a single cylinder optical engine are also reported in this paper. The objective was to apply advanced optical diagnostic techniques to characterize in detail the DF combustion process and provide an improved understanding of this novel combustion strategy and ultimately aid CFD model further developments.

INTRODUCTION

In recent years, increasingly drastic measures have been introduced in order to achieve reductions of IC engine CO₂ and pollutant emissions (*i.e.* HC, CO, NO_x and particulates). In order to comply with the stringent international regulations, automotive engine research will have to focus on the development of advanced combustion strategies. Among the emerging combustion concepts, combining fuels with different ignition and evaporation characteristics has shown interesting potential [1, 2, 3].

The use of an optimized blend of gasoline/diesel fuel can potentially allow improvements of exhaust gas pollutant emissions. The DF concept is based on the ignition of a homogeneous mixture of air (and possibly EGR) and a highly volatile fuel (*i.e.* gasoline, ethanol or natural gas) by injecting a Diesel spray.

Over the past decade, there has been a sustained interest for the DF combustion mode. The majority of DF studies reported in the literature tended to focus on achieving

practical PCCI (Partially Premixed Compression Ignition) or HCCI (Homogeneous Premixed Compression Ignition) operation. The significantly different properties of gasoline and Diesel fuels can provide a means of controlling ignition timing and heat release rate. For example, Bessonette et al. [4] reported that the most suitable fuel for HCCI operation could be a fuel which combines the properties of Diesel and gasoline. Several other investigations have also highlighted the advantages of DF operation on engine performance and identified key parameters such as EGR [5-6], injection strategies [7-8], intake temperature, engine load and fuel reactivity, all of which have an impact on combustion phasing, heat release and pollutant emissions in DF mode.

Jiang et al. [1], Cha et al. [9] and Sauer et al. [10] investigated the effects of the premixed fuel ratio on pollutant emissions and observed that at low engine loads, HC and CO emissions were generally high. However, for gasoline ratios (i.e. gasoline/(gasoline+Diesel fuel)) above 80%, HC and CO emissions decreased to acceptable levels. A decrease in both soot and NO_x emissions was also observed with an increase of the gasoline ratio. In fact, the oxygen concentration is decreased and maximal local temperatures were lower before engine top dead center (TDC). Consequently, the auto-ignition delay, which depends on the amount of fuel, the reaction temperature and the activation energy, was longer and combustion phasing was delayed [2,7]. Using optical engine experiments and numerical simulations, Hanson, Kokjohn et al. [8,11, 12, 13] developed the concept of the reactivity controlled compression ignition (RCCI) concept and showed that DF combustion was sequential and initiated in the more reactive regions within the combustion chamber and moved to the less reactive zones.

A DF concept developed at IFPEN and referred to as In-Cylinder Fuel Blending (ICFB) is based on using port-fuel-injection of gasoline and optimized direct injection of Diesel fuel to control combustion phasing and duration [14]. The engine is operated in Diesel combustion mode at low loads while a DF strategy is employed to operate at high loads. Furthermore, the objective of this strategy is to operate at stoichiometric air fuel ratios using DF combustion which will allow NO_x, HC and CO emissions after-treatment using a three-way catalyst, thereby alleviating the need for more complex and costly exhaust after-treatment systems. The objective was to control exhaust pollutant emissions over the entire engine operating range while maintaining high fuel efficiency.

Despite an increasing interest in the DF concept and the numerous investigations that have been performed in recent years, there is a clear lack of detailed knowledge about the DF combustion process. In particular, determination of the predominant combustion regime(s) and the transition mechanisms between potentially different regimes is crucial for the further optimization of such a concept. In order to achieve a more detailed understanding, different approaches need to be combined which ideally include engine experiments, CFD simulations and optical diagnostic based

engine studies. CFD simulations remain a challenge in the case of DF combustion due to potential contributions from various combustion regimes including auto-ignition, diffusion combustion and possibly premixed flame propagation that might occur.

Current CFD combustion models can help to provide a partial response in terms of identifying different combustion regimes. These approaches are often based on known kinetics of a surrogate fuel whose overall properties in terms of octane and cetane number are similar to those of the real fuel. Part of this study will focus on evaluating the potential of currently available numerical approaches in the CFD code IFP-C3D as a means of characterizing the different combustion regimes and investigation of turbulence effects on such a combustion strategy.

Furthermore, initial results from experiments performed on a single cylinder optical engine are presented. The objective is to apply various diagnostic techniques in order to gain an improved understanding of the DF combustion process and provide valuable data to allow validation of new computational models in the long term.

COMBUSTION MODELS **DESCRIPTION**

Simulations were performed with the MPI parallel solver IFP-C3D [15,16]. This 3D CFD code, devoted to spray and compressible reactive flows modeling, solves the RANS equations using an ALE finite volume method on unstructured hexahedral meshes and a physical time splitting method. Turbulence modeling is achieved with the RNG k- ϵ model [17].

Because of the wide variety of engine configurations, many physical models are used in IFP-C3D to describe the three main combustion modes: Homogeneous auto-ignition (AI), premixed propagation flame and diffusion flame. A unified model, called ECFM3Z (Extended Coherent Flame Model 3 Zones) [18], is implemented in IFP-C3D and coupled with the auto-ignition model TKI [19] to accurately predict these combustion modes as well as abnormal combustion phenomena such as knock.

The ECFM3Z Model

In order to represent the local stratification in the computational cell, the ECFM3Z model takes into account three mixture fraction zones: a pure fuel zone (F), a pure air (plus EGR) zone (A) and a mixed zone (M) (see [Figure 1](#)).

Auto-ignition information is retrieved from the look-up table through linear interpolation along with the following local thermodynamic conditions:

Table 1. TKI look-up table

Variable	Min. value	Max. value	Number of tabulated points
P (MPa)	0.1	20	13
T^u (K)	400	1500	58
φ (-)	0.3	3	6
Y_{res} (-)	0	0.8	4
c_{AI} (-)	0	1	12 (N _p)

The discrete values of $\dot{\omega}_{c,n}^{TKI}$ for the AI progress variable reaction rate to store in the look-up tables are computed as follows

$$\dot{\omega}_{c,n}^{TKI} = \frac{c_{n+1} - c_n}{t_{n+1} - t_n}, \forall n = 1, N_p \quad (9)$$

where c_n and c_{n+1} are the lower and upper bounds of the AI progress variable interval that contains the instantaneous value of c_{AI} , respectively. t_n and t_{n+1} are the instants at which c_n and c_{n+1} are reached during the detailed chemistry calculations, respectively.

The progress variable related to auto-ignition is computed as:

$$c_{AI} = \frac{\tilde{Y}_F^{AI}}{\tilde{Y}_{F^u} + \tilde{Y}_F^{AI}} \quad (10)$$

where \tilde{Y}_F^{AI} is the fuel mass fraction consumed by AI and $\tilde{Y}_{F^u} + \tilde{Y}_F^{AI}$ the maximum value that can be reached by \tilde{Y}_F^{AI} , i.e. the fuel rate likely to be consumed by auto-ignition (since $\tilde{Y}_{F^u} + \tilde{Y}_F^{AI} = \tilde{Y}_{TF} - \tilde{Y}_F^{CFM}$).

Coupling of the Combustion Models

Auto-ignition and flame propagation are two different combustion modes which may interact during knock in spark ignition engines and possibly in the case of Dual Fuel operation. The related models described previously have been coupled in IFP-C3D.

When the ECFM3Z and the TKI models are coupled, the fuel balance equation during combustion writes:

$$\frac{\partial \bar{\rho} \tilde{Y}_{F^u}}{\partial t} + \frac{\partial \bar{\rho} \tilde{u}_i \tilde{Y}_{F^u}}{\partial x_i} = \frac{\partial}{\partial x_i} \left((D + D_i) \frac{\partial \tilde{Y}_{F^u}}{\partial x_i} \right) - \tilde{\omega}_F^{CFM} - \tilde{\omega}_F^{TKI}(c_{AI}) \quad (11)$$

where $\tilde{\omega}_F^{CFM}$ and $\tilde{\omega}_F^{TKI}$ are the source terms due to flame propagation and to auto-ignition, respectively. They are computed as follows

$$\tilde{\omega}_F^{CFM} = \rho^u \tilde{Y}_{TF} S_L \bar{\Sigma} \quad (12)$$

$$\tilde{\omega}_F^{TKI} = \bar{\rho} \tilde{Y}_{TF} \dot{\omega}_c^{TKI}(c_{AI}) \quad (13)$$

When the AI delay is reached, auto-ignition occurs and contributes to the propagation flame by creating a flame surface density due to the spatial heterogeneities of the progress variable. This transition is consequently ensured by:

$$\bar{\Sigma} = |\nabla \tilde{c}| \quad (14)$$

This initialization of $\bar{\Sigma}$ states that the first flame kernels are due only to burnt gases expansion (the stretch effects are not taken into account).

The coupling between the ECFM3Z model and the TKI model has shown to be relevant in the case of knocking in a spark-ignition engine [20] but not been validated in the particular case of Dual Fuel operation.

ENGINE CHARACTERISTICS

Metal Engine Characteristics

In order to evaluate the coupling between the models mentioned above in representative DF conditions, calculations were performed on a single-cylinder Diesel engine configuration and compared to metal engine experiments performed at IFPEN. Table 2 summarizes the engine's main specifications.

Table 2. Engine specifications

Baseline	PSA DW10
Displacement (cm³)	499
Stroke (mm)	88
Bore (mm)	85
Connecting rod length (mm)	145
Compression ratio	14:1
Number of Valves	4
Diesel injection system	Common rail CRI2.2 Bosch
Diesel injection pressure (bar)	1000
Gasoline injection system	Port fuel injection
Gasoline injection pressure (bar)	3
Swirl ratio	1.1

The computational mesh is shown in [Figure 2](#) and only a 60° sector is considered (6-holes injector). One operating point is presented and discussed in the next section. Its main characteristics are presented in [Table 3](#).

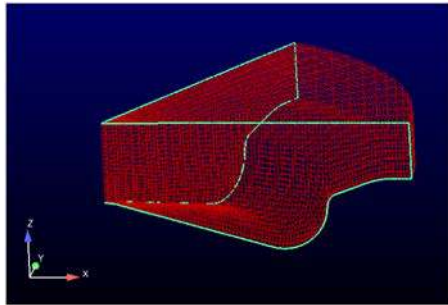


Figure 2. Computational mesh showing the piston-bowl geometry of the PSA DW10 engine

Table 3. Operating point characteristics

SOI (°ATDC)	-20.1
Engine speed (RPM)	2000
EGR rate (%)	29.4
Air flow rate (kg/h)	26.8
Fuel flow rate (kg/h)	1.702
Gasoline ratio (%)	81.1

For simulations, n-heptane is used to represent auto-ignition kinetics of the Diesel fuel and isooctane is the surrogate retained to represent gasoline.

Optical Engine Characteristics and Operating Conditions

Initial experiments on an optically-accessible single cylinder direct-injection Diesel engine have been performed during this study (see [Figure 3](#)). The optical engine has the same geometry as the all-metal engine ([Table 2](#)). The compression ratio was 15:1 and a simplified piston bowl geometry (*i.e.* no bowl pip) was employed. The engine was equipped with a 6-hole injector positioned vertically at the center of the cylinder head. The injector characteristics are given in [Table 4](#).

Table 4. Injector characteristics for optical engine measurements

Number of holes	6
Spray Cone angle	140°
Static flow rate	220ml/30s/100bar

The initial diagnostics performed on the optical engine included high-speed (Photron FASTCAM SA1.1), crank-angle resolved visualization of naturally-occurring combustion luminosity at the frame rate of 36000 images/second.

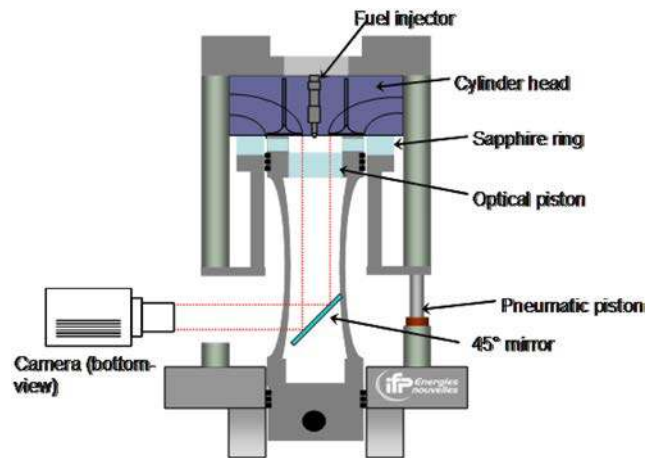


Figure 3. Schematic of the optical engine showing the camera setup for the high-speed combustion luminosity imaging

One important factor taken into account for both the modeling and the optical diagnostic constraints concerns the fuel selection. Since commercial, multi-component fuels are composed of hundreds of compounds, the related fundamental characteristics such as reaction paths, flame velocity, thermodynamic data etc. are not always known. Furthermore the use of commercial fuels for optical engine studies is not always feasible, depending upon the type of diagnostic measurement being performed. This is due to the fact that fluorescent species naturally present within commercial fuels create unwanted background signals and make it difficult to interpret experimental data.

The use of commercial fuels is also challenging for the modeling since developing detailed kinetic schemes is difficult while coupling CFD codes with detailed chemistry models for multi-component fuels is not currently feasible in industrial applications because of the excessive CPU costs. Thus, simplified surrogate fuels must be used. These simplified fuels should ideally be physically and chemically representative of standard, commercial fuels.

For this study, iso-octane was selected to represent gasoline fuel while a blend of iso-octane (36 vol%) and n-decane (64 vol%) was chosen to represent Diesel fuel. The proportions were determined in order to obtain a cetane number of 53 which is comparable to the cetane number of European Diesel. [Table 5](#) shows the properties of the neat compounds and the surrogate Diesel properties.

A comparison of surrogate Diesel with standard commercial Diesel fuel was performed and results are presented subsequently in the paper.

Table 5. N-decane, iso-octane, and surrogate Diesel properties

	N-decane	Iso-octane	Surrogate Diesel
Molar mass (g/mol)	142.28	114.23	131.07
Density (kg/m³)	726	692	713.76
LHV (MJ/Kg)	44.24	44.31	44.26
RON	-41	100	9.76
MON	-38	100	11.68
Cetane number	76	12	52.96

The engine operating conditions are shown in [Table 6](#) for the DF conditions studied on the optical engine.

Table 6. Engine operation under optical engine experiments

Engine speed	1200 rpm
Intake temperature	40°C
Intake pressure	0.7 bar
Direct injection pressure	400 bar
Direct injection SOI	14° BTDC
Direct injection DOI	400 μs

The current paper presents preliminary results of optical engine experiments including an overall equivalence ratio sweep which was performed by varying the premix fuel rate in order to characterize different combustion regimes (The iso-octane ratio varied from 87% to 90% without charge dilution and from 87 to 92% when using N₂ dilution). The equivalence ratio sweep reported in this paper was performed with and without charge dilution. Intake charge dilution was performed by using pure N₂ as synthetic EGR which was mixed with the intake air. Results are presented for cases without charge dilution and with 13% N₂. [Table 7](#) shows the fuel mixture properties and the IMEP of the selected experimental points.

Table 7. Equivalence ratios and IMEP for the operating conditions without and with charge dilution

0% N ₂				
Global equivalence ratio	0.49	0.59	0.69	
Premixed fuel ratio (%)	87	89	90	
IMEP (bar)	2.9	3.5	4.0	
13% N ₂				
Global equivalence ratio	0.56	0.73	0.84	0.96
Premixed fuel ratio (%)	87	90	91	92
IMEP (bar)	2.1	1.7	2.2	2.5

RESULTS AND DISCUSSION

Evaluation of Combustion Models on a Dual Fuel Application

[Figure 4](#) shows the experimental and predicted cylinder pressure:

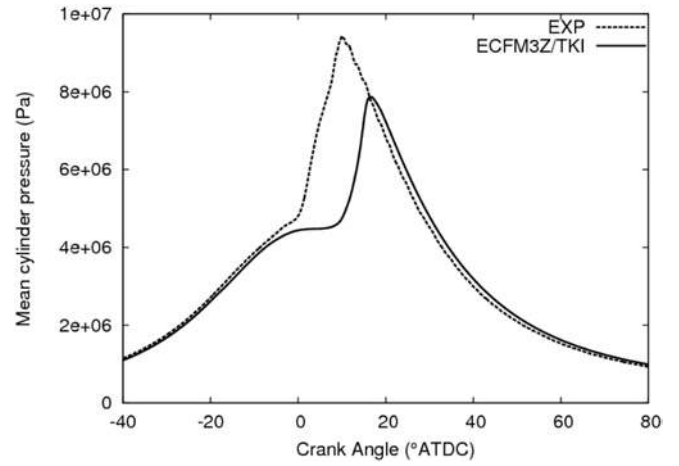


Figure 4. Comparison of experimental (dashed lines) and predicted (solid lines) mean cylinder pressure - SOI = 21° BTDC - Computations were performed with the ECFM3Z/TKI coupling

The predicted mean cylinder pressure is not in a good agreement with the experimental one. Indeed, combustion phasing and intensity are not well reproduced.

The global reaction rate of combustion as well as those related to auto-ignition (AI), burned gas post-oxidation (BG) and flame propagation (ECFM - Extended Coherent Flame Model), are computed respectively as follows and plotted in [Figure 5](#):

$$\dot{\omega}_{Global} = \frac{\rho_F^{n+1} - \rho_F^n}{\Delta t} \quad (15)$$

$$\dot{\omega}_{AI} = \left(\frac{\rho_F^{n+1} - \rho_F^n}{\Delta t} \right)_{AI} \quad (16)$$

$$\dot{\omega}_{BG} = \left(\frac{\rho_F^{n+1} - \rho_F^n}{\Delta t} \right)_{BG} \quad (17)$$

$$\dot{\omega}_{ECFM} = \left(\frac{\rho_F^{n+1} - \rho_F^n}{\Delta t} \right)_{ECFM} \quad (18)$$

where ρ_F is the mean density in the combustion chamber, Δt the time step, n and $n+1$ the indices of the present and the next instants respectively.

This representation aims to evaluate the contribution of each combustion model to the global reaction rate which writes:

$$\dot{\omega}_{Global} = \dot{\omega}_{AI} + \dot{\omega}_{BG} + \dot{\omega}_{ECFM} \quad (19)$$

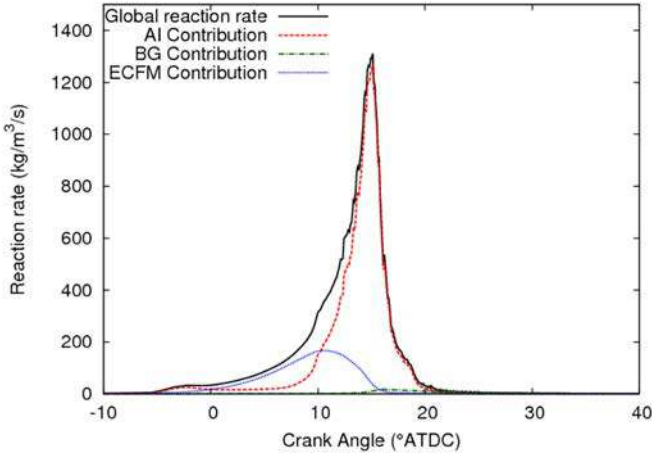


Figure 5. Contribution of each combustion model to the global reaction rate - SOI= 20.1° BTDC - Computations were performed with the ECFM3Z/TKI coupling

Auto-ignition starts at 5° BTDC. In this first-stage combustion, the local stratification of the progress created by AI initializes the flame surface density. The propagation model is activated and its contribution to the global reaction rate is significant. During the second-stage combustion, the auto-ignition delay is reached and the main heat release is due to AI. This first modeling of the transition between the two combustion regimes given by Eq. (13) leads to an underestimation of the overall reaction rate.

To better characterize the initialization of the premixed flame by auto-ignition process, the equilibrium flame stretch ki_{eq} is introduced in the initial flame surface density calculation. This approach relies on the basic ideas proposed by Colin et al. [23,24] to take into account the turbulence effects on the initial flame surface density deposition for spark-ignition engines. An expression for ki_{eq} is given by:

$$ki_{eq} = 1 + \frac{2}{S_L} \sqrt{\alpha K_t \tau_t \frac{k^2}{\varepsilon}} \quad (20)$$

where αK_t is the flame surface stretch due to turbulence, τ_t the turbulence characteristic time, k the turbulent kinetic energy and ε the dissipation rate.

The new flame surface density initial deposit takes into account the turbulence effects on the flame surface:

$$\bar{\Sigma} = ci_{eq} ki_{eq} |\nabla \tilde{c}| \quad (21)$$

where ci_{eq} is a parameter that varies between 0 and 1. It is used to control the transition between the models and the contribution of the turbulent stretch to the initial flame kernel.

Figure 6 shows a comparison between the experimental and the computed (ECFM3Z/TKI with $ci_{eq} * ki_{eq}$ (red) and ECFM3Z/TKI with ki_{eq} (green)) mean cylinder pressures.

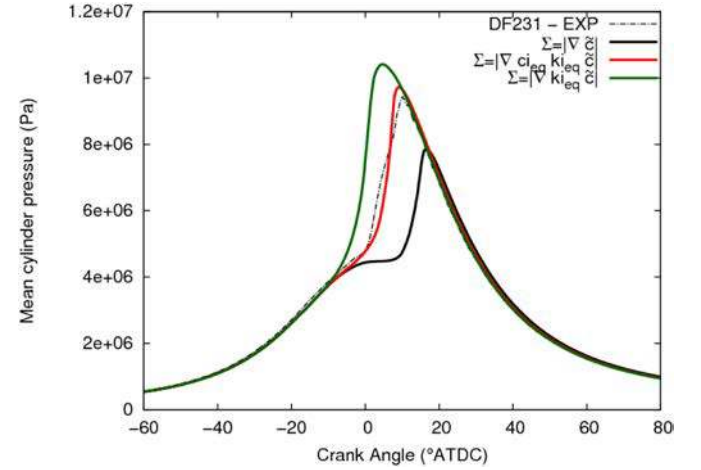


Figure 6. Comparison of experimental (dashed lines) and predicted (solid lines) mean cylinder pressures - Computations were performed with the ECFM3Z/TKI coupling and took into account the equilibrium turbulence stretch

It appears that the Dual Fuel modeling is very sensitive to the transition between combustion regimes. When the stretch effects are fully taken into account in the initial kernel growth, combustion starts before TDC and maximum pressure is overestimated. However, the use of the control parameter shows a better description of the combustion process. Indeed, combustion phasing is well reproduced and a better estimation of the combustion intensity and duration is performed. Taking into account the turbulent stretch effect is a relevant choice to describe the initial flame growth after auto-ignition occurs. But in order to realize an optimal coupling between combustion models, it's crucial to determine a more physical criterion.

Figure 7 represents the reaction rates logarithmic scale computed with the ki_{eq} contribution. The auto-ignition model initializes the flame propagation and the latter pilots the combustion until the AI delay is reached. The main heat release is realized by the auto-ignition process as we can see it in Figure 8.

To better understand the transition between combustion regimes and the contribution of each combustion model, in-cylinder images from the modeling work are presented. Figures 9, 10, 11, 12, 13 show cut planes coincident with the spray axis and colored by AI and CFM reaction rates and by temperature, and flame surface density due to auto-ignition (to identify spatially the beginning of combustion) in Figure 9.

The Diesel fuel is injected in the combustion chamber at 20.1° BTDC. It evaporates and auto-ignition starts locally

(Figure 9). The progress variable gradient generated then initializes the first propagation flame kernel.

At 4° BTDC, combustion is located at the periphery of the combustion chamber and is mainly controlled by the propagation model (see Figure 10). Auto-ignition still occurs at the downstream region of the evaporated spray.

Figure 11 shows “pockets” of auto-ignition. These localized AI sites suggest that the AI process ignites the premixed air/isooctane. The created flame propagates towards the center of the chamber and sweeps the auto-ignition front. The same observation can be made at top dead center (Figure 12) and at 2° ATDC (Figure 13) where the main heat release is reached.

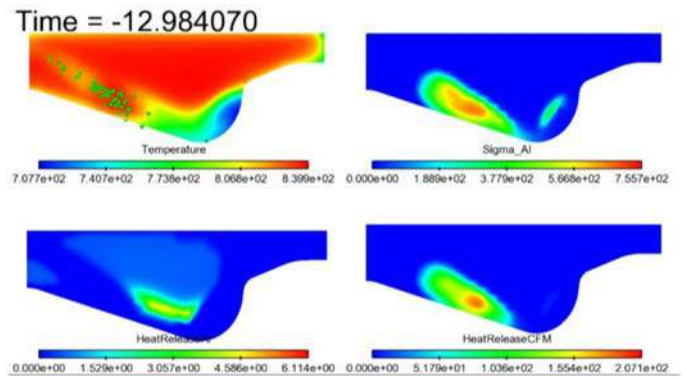


Figure 9. Cut planes of temperature, flame surface density due to auto-ignition, AI and CFM reaction rates at -13°ATDC (DF3)

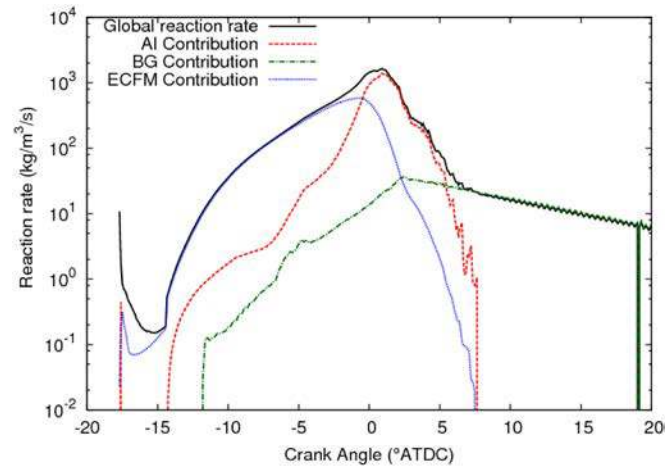


Figure 7. Contribution of every combustion model to the global reaction rate in logarithmic scale - SOI= 20.1° BTDC - Computations were performed with the ECFM3Z/TKI coupling and took into account the equilibrium turbulence stretch

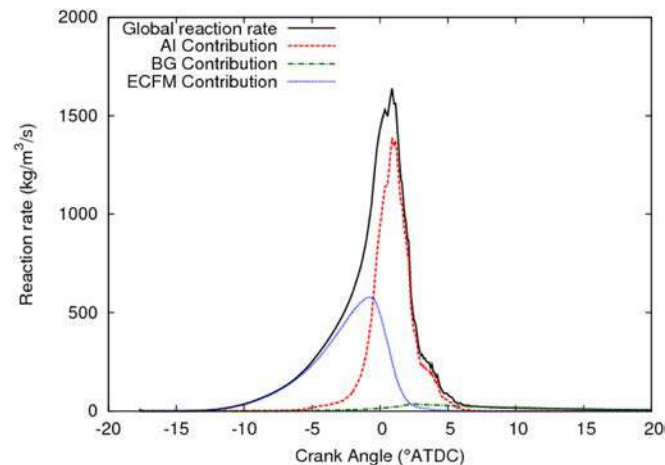


Figure 8. Contribution of every combustion model to the global reaction rate - SOI= 20.1° BTDC - Computations were performed with the ECFM3Z/TKI coupling and took into account the equilibrium turbulence stretch (KIEQ)

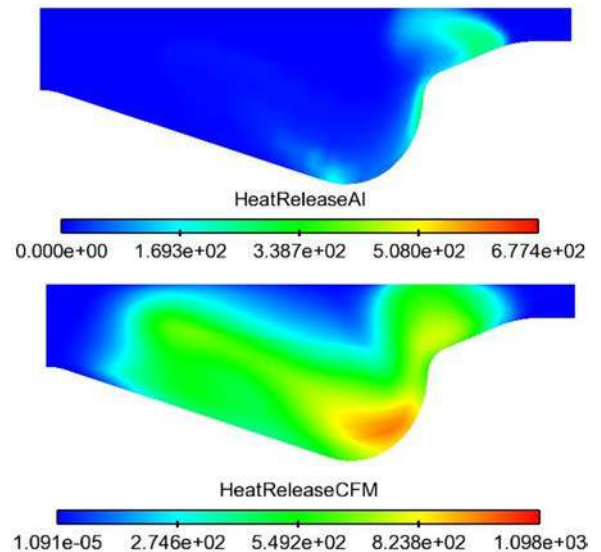


Figure 10. Cut planes of AI and CFM reaction rates at 4° BTDC

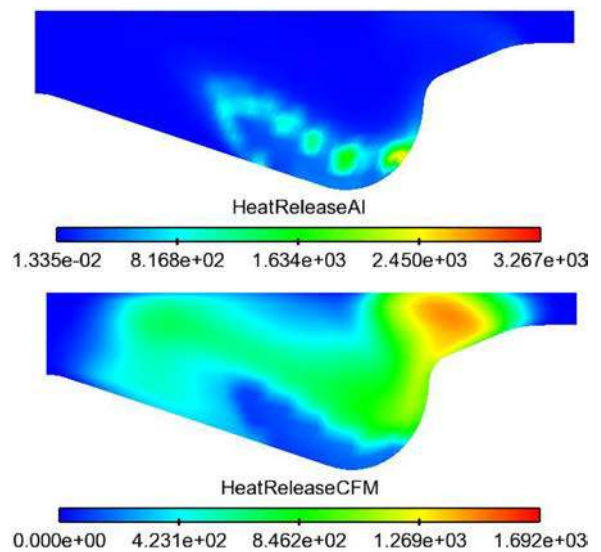


Figure 11. Cut planes of AI and CFM reaction rates at 2° BTDC

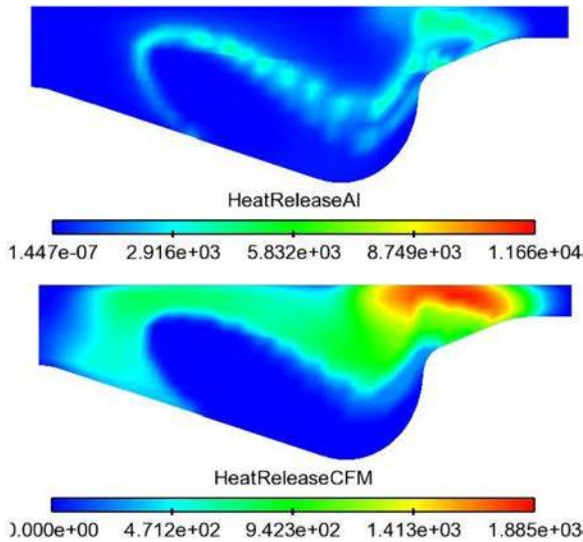


Figure 12. Cut planes of AI and CFM reaction rates at top dead center

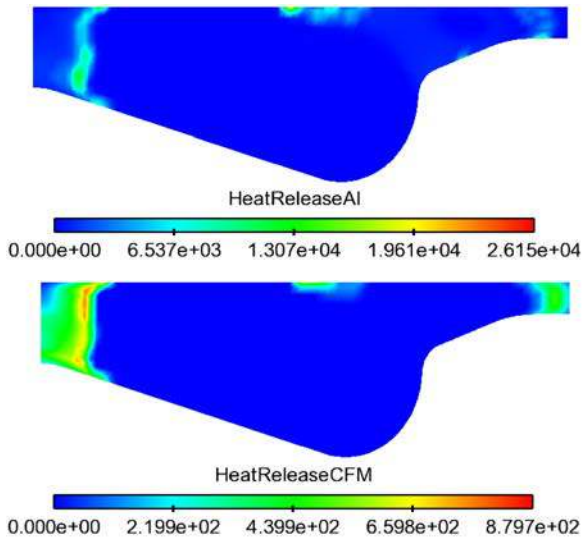


Figure 13. Cut planes of AI and CFM reaction rates at 2° ATDC

Optical Engine Experiments

The first experiments performed in DF mode on the optical engine were to validate the Diesel surrogate fuel blend (the Diesel surrogate fuel is hereafter referred to as GMA) by performing a back-to-back comparison with standard commercial Diesel. Figures 14 and 15 show a comparison between conventional Diesel fuel and the GMA blend in terms of cylinder pressure and heat release rate for both fuels tested on the optical engine.

At a low load condition, i.e. 3.2 bar IMEP (Figure 14), although the AI delay of GMA is comparable with Diesel, a higher pressure-rise rate is observed for GMA. This may be explained by the higher volatility of GMA compared to Diesel fuel which would tend to increase the proportion of premixed fuel consumed during the combustion process.

At a mid-load condition (1200 rpm, 7 bar IMEP), the GMA and Diesel fuel reveal overall satisfactory agreement (see Figure 15) in terms of AI delay and combustion phasing although the pressure-rise rate appears to be slightly higher for GMA leading to marginally higher peak in-cylinder pressures.

Despite slight differences observed between the GMA blend and standard Diesel, the results confirmed that the model fuel (GMA) are overall representative of Diesel fuel in terms of ignition timing and combustion phasing.

The dual fuel experiments were performed with a global equivalence ratio sweep from 0.49 to 0.69 without charge dilution and from 0.56 to 0.96 with 13% N₂. Experiments were not performed at higher equivalence ratios in order to avoid excessive pressure-rise rates. Figure 16 and 17 display respectively mean in-cylinder pressures and the apparent rate of heat release, for three equivalence ratios without charge dilution. The quantity of Diesel fuel injection was maintained constant for the equivalence ratio sweep while the premixed fuel quantity (i.e. quantity of iso-octane) was increased progressively. As equivalence ratio increases, the heat release characteristics are significantly modified.

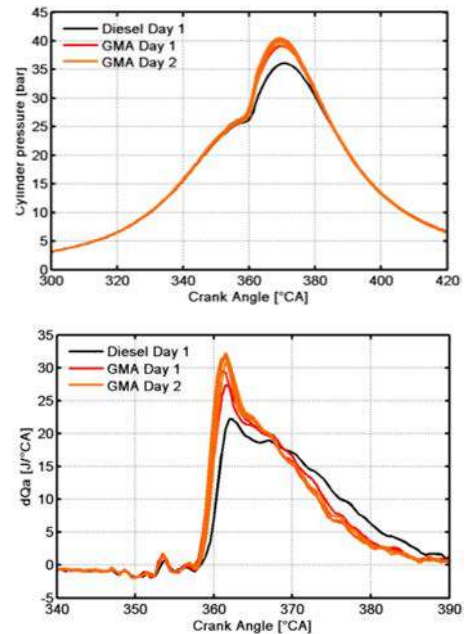


Figure 14. Mean cylinder pressure (upper graph) and heat release rate (lower graph) at low load - Engine speed = 1200 rpm - Equivalence ratio=0.6 - 0% EGR - SOI = 10 BTDC - DOI = 400 μ s - P_{inj} = 400 bar - P_{int} = 0.7 bar - T_{int} = 40°C

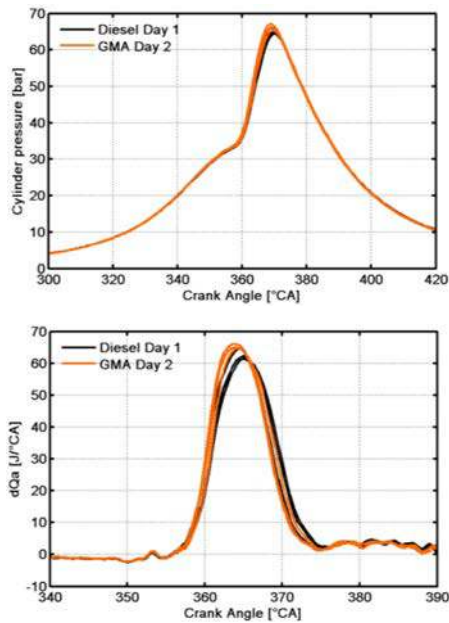


Figure 15. Mean cylinder pressure (upper graph) and heat release rate (lower graph) at mid load (7 bar IMEP) - Engine speed = 1200 rpm - Equivalence ratio=0.9 - 15% N₂ - SOI = 10 BTDC - DOI = 400 μ s - Pinj = 400 bar - Pint = 0.9 bar - Tint = 40°C

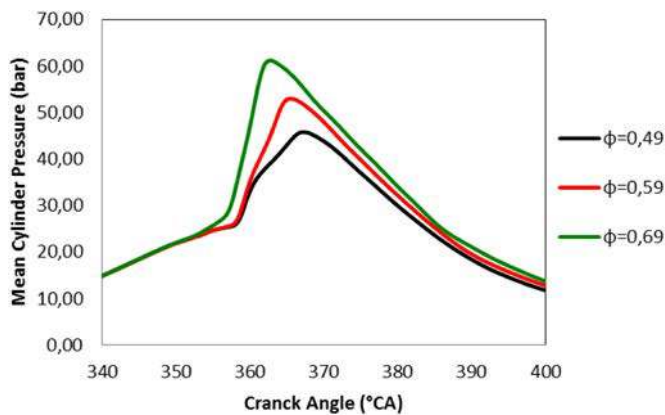


Figure 16. Mean cylinder pressure for the equivalence ratio sweep - 0% N₂

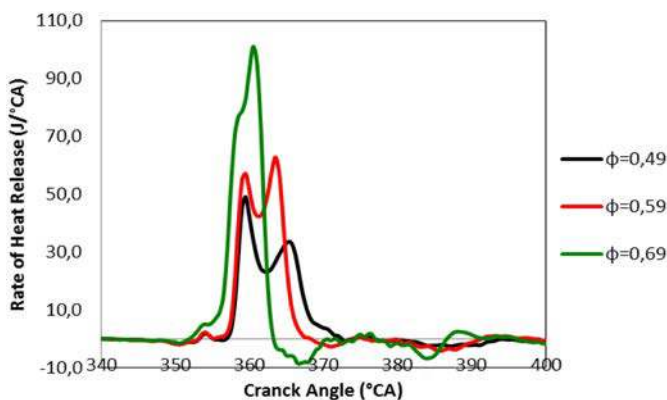


Figure 17. Rate of heat release for the equivalence ratio sweep - 0% N₂

In [Figure 17](#), a first small peak is observed near 6° BTDC most likely due to the cool flame produced by the initial oxidation of decane present in the surrogate Diesel (since iso-octane is a single-stage fuel). Combustion is clearly highly sensitive to fuel reactivity. For the condition where the global equivalence ratio is below 0.6, the rate of heat release is characterized by 2 major peaks, the first occurring at TDC, which is the result of Diesel fuel auto-ignition in the downstream regions of the evaporated sprays, located in the periphery of the bowl. The second peak occurs a few degrees after TDC. An increase in overall equivalence ratio to above 0.6 results in a shorter ignition delay and the rate of heat release is characterized by a single peak and a shorter combustion duration.

[Figure 18](#) and [19](#) display respectively mean in-cylinder pressures and the apparent rate of heat release, for four equivalence ratios with 13% N₂ dilution. Intake charge dilution significantly modifies overall combustion behavior with an expected increase of the auto ignition delay. Dilution of the intake charge reduces overall oxygen concentration and thereby modifies mixture reactivity.

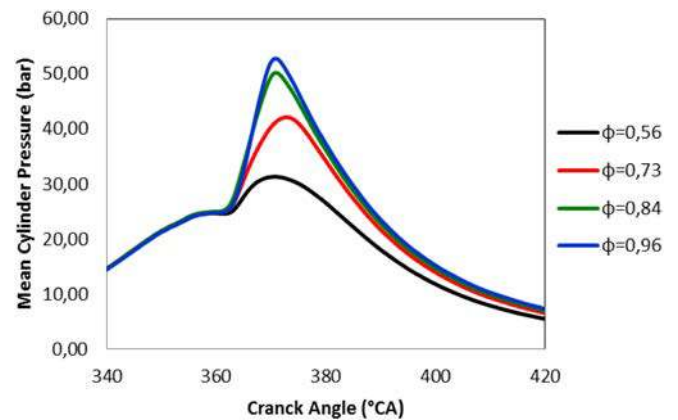


Figure 18. Mean cylinder pressure for the equivalence ratio sweep - 13% N₂

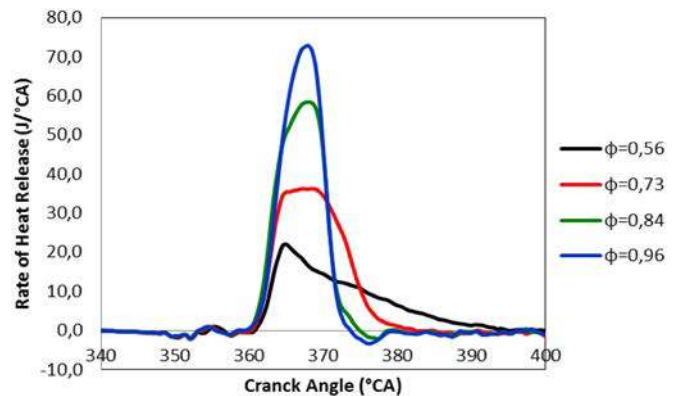


Figure 19. Rate of heat release for the equivalence ratio sweep - 13% N₂

For the equivalence ratio condition of 0.56 (same premixed fuel ratio as the first point with no EGR dilution), the heat release rate is characterized by a single peak at 5° ATDC

followed by a relatively slow heat release phase until approximately 35° ATDC. This latter phase appears analogous to diffusion-limited Diesel combustion and suggests that the main heat release is principally a result of auto-ignition of the surrogate Diesel injection which entrains a premixed charge of iso-octane/air into the fuel jet.

Figure 20 shows recorded images of combustion natural luminosity at $\phi=0.56$ at different crank angle positions. The imaging data reveals that combustion starts after TDC predominantly in the periphery of the combustion chamber, in the zones where the spray is expected to impinge on the piston bowl wall. The combustion images do not reveal the presence of signal in the central region of the bowl, indicating that the premixed fuel within this zone will likely not be consumed at such low equivalence ratios.

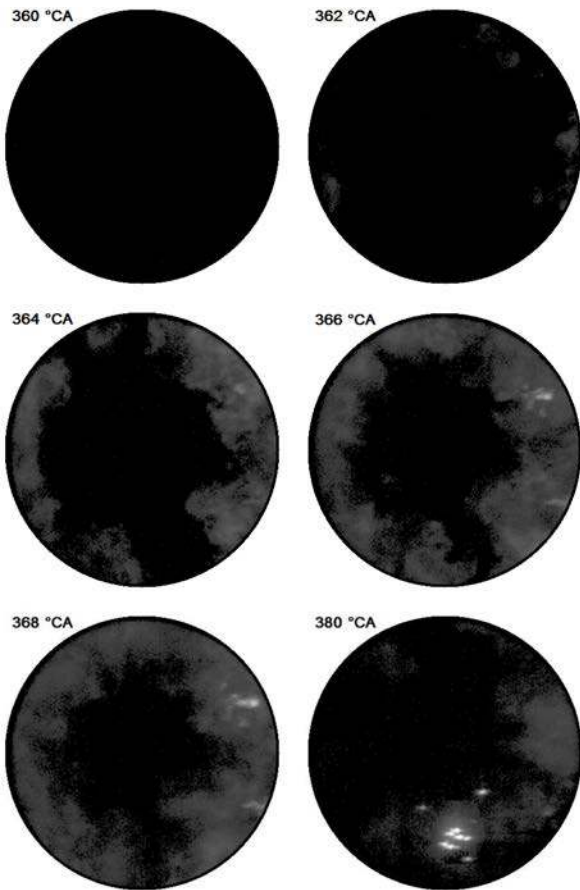


Figure 20. High speed camera images of Dual Fuel combustion at $\phi=0.56$ – 13% EGR

At higher equivalence ratios, combustion behavior differs significantly. Figures 18 and 19 reveal higher pressure rise rates and more notably, a bell-like single-peak heat release for equivalence ratios of 0.73 and above. As can be seen in Figure 21, 2° ATDC, auto-ignition pockets are located at the periphery of the combustion chamber and gradually move to the center (at 6 and 8° ATDC). High speed movies revealed a rapid motion of burned gases in the center of the chamber which corresponds temporally with the main heat release peak. Although it remains to be quantified, the high speed

images suggest that this second-stage combustion could be a result of mass auto-ignition of the remaining premixed fuel. The mechanisms responsible for the reaction zone to extend from the periphery to the central part of the bowl have not yet been determined although it is believed to be due to sequential auto-ignition of the premixed charge as a result of the increasingly higher in-cylinder temperatures or possibly the result of premixed flame propagation or a combination of both these combustion modes. The combustion luminosity images shown in Figure 21 reveal that the combustion zone extends from the bowl periphery to the central region of the bowl, leading to increased consumption of the premixed iso-octane in the central part of the chamber.

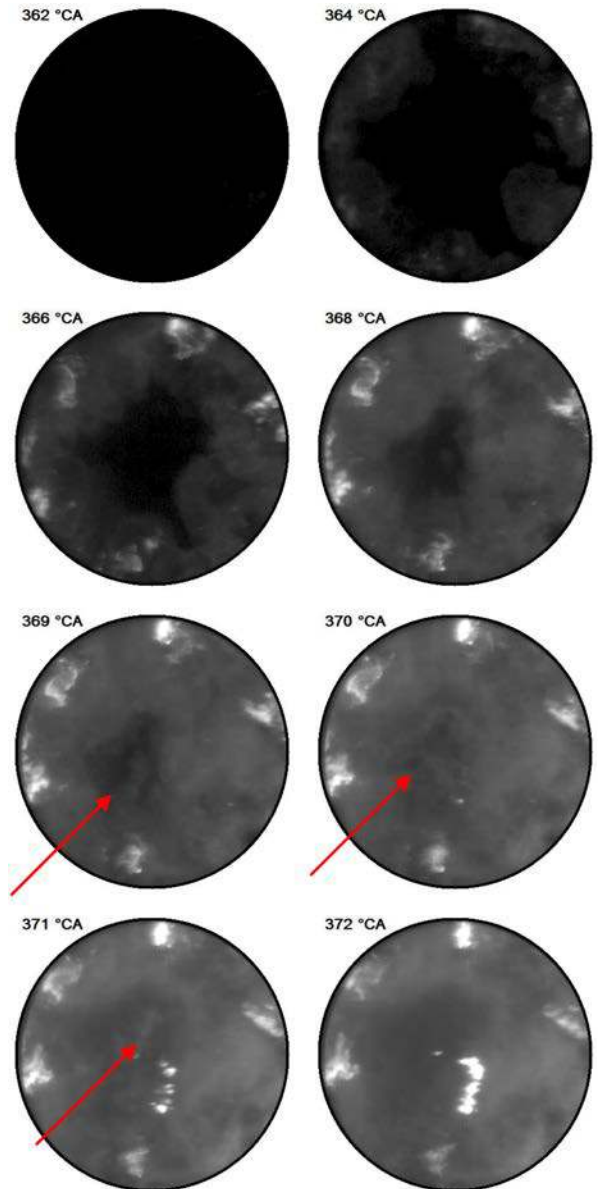


Figure 21. High speed camera images of Dual Fuel combustion at $\phi=0.73$

CONCLUSIONS

A first evaluation of the coupling between a turbulent combustion model for flame propagation in stratified mixtures (ECFM3Z) and a tabulated kinetics model for auto-ignition (TKI) was conducted in order to achieve a better understanding of the Dual Fuel combustion strategy. A criterion for the transition between the different combustion regimes was adopted based on the initial flame surface density deposition. An evaluation in real engine conditions has enabled identification of the predominant regime during the engine cycle and to represent the heat release distribution inside the chamber.

The turbulence stretch was then added to the model taking into account turbulent effects on the initial flame surface growth. It showed a faster transition between auto-ignition and flame propagation. The predicted combustion velocity is overestimated compared to experimental reference and presents a one-stage process. It was shown that the results are sensitive to the transition between the combustion regimes.

Representative fuels were selected and characterized experimentally in view of comparisons between experiments and engine CFD simulations. Initial optical engine experiments were performed and high speed imaging of the naturally-occurring combustion luminosity revealed notable variations in combustion behavior as a function of overall equivalence ratio. Although more detailed diagnostics will be performed by the authors in the future, including tracer LIF and OH LIF measurements, these first results reveal a notable effect on heat release rate. Although it remains to be confirmed, imaging data appear to reveal initial auto-ignition of the premixed charge occurring as a result of the pilot Diesel injection followed by a sequential auto-ignition of the remaining, predominantly premixed charge or by flame propagation or a combination of these combustion regimes.

Further improvements are needed to ensure a better description of the transition between the different combustion models. In the near future the objective will be to adopt a different mixing model, based on a presumed PDF and a new transition criterion will be also taken into account. Experimental investigations on the optical engine will continue with the application of more detailed diagnostic techniques which will support a more extensive validation of the numerical simulations.

REFERENCES

1. Jiang, H., Wang, J., and Shuai, S., "Visualization and Performance Analysis of Gasoline Homogeneous Charge Induced Ignition by Diesel," SAE Technical Paper [2005-01-0136](#), 2005, doi:[10.4271/2005-01-0136](#).
2. Inagaki, K., Fuyuto, T., Nishikawa, K., Nakakita, K. et al., "Dual-Fuel PCI Combustion Controlled by In-Cylinder Stratification of Ignitability," SAE Technical Paper [2006-01-0028](#), 2006, doi:[10.4271/2006-01-0028](#).

3. Kokjohn, S., Hanson, R., Splitter, D., and Reitz, R., "Experiments and Modeling of Dual-Fuel HCCI and PCCI Combustion Using In-Cylinder Fuel Blending," *SAE Int. J. Engines* 2(2):24-39, 2009, doi:[10.4271/2009-01-2647](#).
4. Bessonette, P., Schleyer, C., Duffy, K., Hardy, W. et al., "Effects of Fuel Property Changes on Heavy-Duty HCCI Combustion," SAE Technical Paper [2007-01-0191](#), 2007, doi:[10.4271/2007-01-0191](#).
5. Han, X., Xie, K., Zheng, M., and De Ojeda, W., "Ignition Control of Gasoline-Diesel Dual Fuel Combustion," SAE Technical Paper [2012-01-1972](#), 2012, doi:[10.4271/2012-01-1972](#).
6. Leermakers, C., Van den Berge, B., Luijten, C., Somers, L. et al., "Gasoline-Diesel Dual Fuel: Effect of Injection Timing and Fuel Balance," SAE Technical Paper [2011-01-2437](#), 2011, doi:[10.4271/2011-01-2437](#).
7. Tamagna, D., Gentili, R., Ra, Y., and Reitz, R., "Multidimensional Simulation of the Influence of Fuel Mixture Composition and Injection Timing in Gasoline-Diesel Dual-Fuel Applications," SAE Technical Paper [2008-01-0031](#), 2008, doi:[10.4271/2008-01-0031](#).
8. Hanson, R., Kokjohn, S., Splitter, D., and Reitz, R., "An Experimental Investigation of Fuel Reactivity Controlled PCCI Combustion in a Heavy-Duty Engine," *SAE Int. J. Engines* 3(1):700-716, 2010, doi:[10.4271/2010-01-0864](#).
9. Cha, J., Kwon, S., and Park, S., "An experimental and modeling study of the combustion and emission characteristics for gasoline-diesel dual-fuel engines", Proceedings Of The Institution Of Mechanical Engineers Part D-Journal Of Automobile Engineering, 225(D6), 2011.
10. Sauer, C., Schneemann, A., Teetz, C., Bach, F., et al., "HCCI in off-Highway-Engines as an Alternative to meet Future Emission Legislation", 2011.
11. Kokjohn, S., Hanson, R., Splitter, D., and Reitz, R., "Experiments and Modeling of Dual-Fuel HCCI and PCCI Combustion Using In-Cylinder Fuel Blending," *SAE Int. J. Engines* 2(2):24-39, 2009, doi:[10.4271/2009-01-2647](#).
12. Hanson, R., Kokjohn, S., Splitter, D., and Reitz, R., "Fuel Effects on Reactivity Controlled Compression Ignition (RCCI) Combustion at Low Load," *SAE Int. J. Engines* 4(1): 394-411, 2011, doi:[10.4271/2011-01-0361](#).
13. Splitter, D., Hanson, R., Kokjohn, S., and Reitz, R., "Reactivity Controlled Compression Ignition (RCCI) Heavy-Duty Engine Operation at Mid-and High-Loads with Conventional and Alternative Fuels," SAE Technical Paper [2011-01-0363](#), 2011, doi:[10.4271/2011-01-0363](#).
14. Duffour, F., Ternel, C., and Pagot, A., "IFP Energies Nouvelles Approach for Dual Fuel Diesel-Gasoline Engines," SAE Technical Paper [2011-24-0065](#), 2011, doi:[10.4271/2011-24-0065](#).
15. Bohbot, J., Gillet, N., and Benkenida, A., "IFP-C3D : an Unstructured Parallel Solver for Reactive Compressible Gas Flow with Spray". *Oil & Gas Science and Technology - Rev. IFP*, 64(3), June 2009.

16. Velghe, A., Gillet, N., Bohbot, J., “A high efficiency parallel unstructured solver dedicated to internal combustion engine simulation”, *Computers & Fluids*, Volume 45, Issue 1, June 2011, doi:[10.1016/j.compfluid.2011](https://doi.org/10.1016/j.compfluid.2011).

17. Han, Z., Reitz, R., “Turbulence modeling of internal combustion engines using RNG k- ϵ models,” *Combustion Science and Technology*, 1995, doi:[10.1080/00102209508907782](https://doi.org/10.1080/00102209508907782).

18. Colin, O., and Benkenida, A., “The 3-Zones Extended Coherent Flame Model (ECFM3Z) for Computing Premixed/Diffusion Combustion,” *Oil & Gas Science and Technology - Rev. IFP*, 59(6) :593-609, 2004

19. Colin, O., Pires, Da Cruz, A., and Jay, S., “Detailed Chemistry-based Auto-ignition Model Including Low Temperature Phenomena Applied to 3D Engine Calculations,” *Proc Combust Inst*, 2649-2656, 2005.

20. Colin, O., Benkenida, A., and Angelberger, C., “3D Modeling of Mixing, Ignition and Combustion Phenomena in Highly Stratified Gasoline Engines”, *Oil & Gas Science and Technology - Rev. IFP*, 58(1) :47-62, 2003.

21. Metghalchi M, Keck JC. Burning velocities of mixtures of air with methanol, isooctane, and indolene at high pressure and temperature. *Combust Flame* 1982;48:191-210.

22. Knop, V., Michel, J-B., and Colin, O., “On the Use of a Tabulation Approach to Model Auto-Ignition During Flame Propagation in SI Engines”, 156 :505-521, 2009.

23. Duclos, J.M., and Colin, O., “Arc and Kernel Tracking Ignition Model for 3D Spark-Ignition Engine Calculation”, 2001.

24. Colin, O. and Truffin, K, “A Spark Ignition Model for Large Eddy Simulation Based on an FSD Transport Equation (ISSIM-LES)”, *Proceedings of the Combustion Institute*, 33 : 3097-3104, 2011.

DEFINITIONS/ABBREVIATIONS

DF - Dual Fuel

ICFB - In-Cylinder Fuel Blending

HCCI - Homogeneous Charge Compression Ignition

PCCI - Premixed Charge Compression Ignition

RCCI - Reactivity Controlled Compression Ignition

CFD - Computational Fluid Dynamics

CPU - Central processing unit

ATDC - After Top Dead Center

BTDC - Before Top Dead Center

ALE - Arbitrary Lagrangian Eulerian

RANS - Reynolds Averaged Navier-Stokes

FSD - Flame Surface Density

ECFM3Z - Extended Coherent Flame Model 3 Zones

TKI - Tabulated Kinetics of Ignition

AI - Auto-Ignition

EGR - Exhaust Gas Recirculation

RPM - Revolution Per Minute

SOI - Start Of Injection

DOI - Duration Of Injection

PDF - Probability Distribution Function

ACKNOWLEDGMENTS

This work was supported by IFPEN. The authors are grateful to Nicolas Dronniou for his suggestions and advice during the experiments.